ChemPubSoc Europe

DOI: 10.1002/cctc.201600429

CHEMCATCHEM Communications

Enhanced Electrokinetics of C–C Bond Splitting during Ethanol Oxidation by using a Pt/Rh/Sn Catalyst with a Partially Oxidized Pt and Rh Core and a SnO_2 Shell

Guangxing Yang,[a] Anatoly I. Frenkel,[b, c] Dong Su,[d] and Xiaowei Teng*[a]

Direct ethanol fuel cells (DEFCs) are a promising technology for generating electricity through the electro-oxidation of liquid ethanol. Its implementation requires the development of anode catalysts capable of producing CO_2 and yielding 12-electron transfer through breaking the C–C bond of ethanol. Here, we presented comprehensive studies of the electrokinetics of CO_2 generation on Pt/Rh/Sn ternary catalysts. Our studies showed that the triphasic $PtRhO_x$–SnO_2 catalysts with a partially oxidized Pt and Rh core and a SnO_2 shell, validated by X-ray absorption analyses and scanning transmission electron microscope-electron energy loss spectroscopy line scans, coincided with a 2.5-fold increase in the CO_2 generation rate towards ethanol oxidation reaction, compared with the biphasic PtRh-SnO_2 catalysts with a metallic PtRh alloy core and commercial Pt. These studies provided insight into the design of a new genre of electrocatalysts with a partially oxidized noble metal.

Energy demands coupled with concerns over environmental pollution have created a great need for clean and efficient power sources. Fuel cells that enable the direct conversion of chemical energy to electricity with over 90% thermodynamic efficiency become viable alternative power devices to internal combustion engines where thermodynamic efficiency is subject to the Carnot cycle limitation (typically $<35\%$). Ethanol, recognized as a substantial energy source in the green technologies, has many advantages over hydrogen gas as a fuel in fuel cells: ethanol has a lower toxicity, a high boiling point for safer storage in transportation applications, a great availability from fermenting sugar-containing and/or cellulose-containing raw materials, and the established infrastructure for production and distribution. In recent years, direct ethanol fuel cells (DEFCs) have been extensively studied, with peculiar attention to their anode reactions, namely the ethanol oxidation reaction (EOR). Ethanol is the simplest molecule containing C–C, C–H, C–O, and O–H bonds, and the selective cleavage of these bonds determines the reaction pathways and relative selectivity of products. For example, EOR through the C–C bond-cleavage pathway leads to the production of CO_2 through a complete oxidation of ethanol with a twelve-electron transfer, whereas cleavage of the C–H, O–H, and/or C–O bonds without the C–C bonds lead to incomplete oxidation with production of acetaldehyde (two-electron transfer) or acetic acid (four-electron transfer).[1–6]

Biphasic PtRh–SnO_2 materials with a PtRh alloy and a segregated SnO_2 phase have been considered as the best catalyst for EOR owing to their high reactivity for adsorption, dehydrogenation, and oxidation of ethanol by C–C splitting, as well as plausible chemical stability.[7–14] The superiority of Pt and Rh towards C–C splitting has been demonstrated by density functional theory (DFT) calculations, showing that Pt–Rh help cleave the C–H bond of the terminal methyl group (β-carbon dehydrogenation) and form oxometallate intermediates (M-CH_2-CH_2-O-M).[15] Oxophilic Sn, on the other hand, interacts with water strongly to form an oxygenated species on the catalyst surface (OH_{ads}), which helps oxidize the reaction intermediates (e.g., CH_x and CO) generated on adjacent Pt or Rh sites.[16,17] Attributed to this bifunctional effect, Pt/Rh/Sn ternary catalysts have been generally considered as the most effective materials for the EOR, especially at higher overpotentials. However, fuel cells generally tend to operate at an external potential close to their equilibrium potential. At low overpotentials at the anode, the Pt/Rh/Sn components have a weak dissociative adsorption of water, and the resulting low OH_{ads} coverage on the catalyst surface may not be adequate to remove the strongly adsorbed reaction intermediates, especially CO, which poisons the active sites. Therefore, finding an optimal catalytic structure that can effectively dissociate ethanol by C–C splitting at low overpotentials and consequently remove the CO intermediates is of great importance for the implementation of DEFC technology.

In the past decade, studies have shown that the kinetics of the CO oxidation reaction on surfaces of Ru, Pt, Pd, Rh, and PtRh increases significantly in conjunction with the formation of a thin oxide film on the surface of the metal or alloy

[a] G. Yang, Prof. X. Teng
Department of Chemical Engineering
University of New Hampshire
NH 03824 (USA)
E-mail: xw.teng@unh.edu

[b] Prof. A. I. Frenkel
Department of Physics
Yeshiva University
NY 10016 (USA)

[c] Prof. A. I. Frenkel
Present address: Department of Materials Science and Chemical Engineering
Stony Brook University
NY 11794 (USA)

[d] Dr. D. Su
Center for Functional Nanomaterials
Brookhaven National Laboratory
NY 11973 (USA)

Supporting information and the ORCID identification number(s) for the author(s) of this article can be found under http://dx.doi.org/10.1002/cctc.201600429.

catalysts.[18–22] It has been found that the active phase for CO oxidation is oxidized rather than metallic. Although these results obtained from solid/gas-phase reactions are expected to be relevant for general heterogeneous catalysis, the reactivity of noble metal oxides towards electrocatalysis, especially EOR, has not been well studied. Particularly, most of the studies on Pt-based EOR catalysts have only been focused on non-noble metal oxides, such as SnO_2 and CeO_2.[17,23] However, the role of Pt or Rh oxides on the electrokinetics of EOR, especially the C–C splitting, has not been reported.

In this study, we synthesized two types of carbon supported Pt/Rh–SnO_2 core–shell nanoparticles: one was triphasic $PtRhO_x$–SnO_2 with a partially oxidized Pt and Rh core (segregated Pt and Rh phases) and a SnO_2 shell, and the other was biphasic PtRh–SnO_2 with a PtRh alloy core and a SnO_2 shell. By using our newly designed four-electrode electrochemical cell equipped with a CO_2 microelectrode, we comprehensively studied the electrokinetics of CO_2 generation, including the CO_2 generation rate and CO_2 selectivity, with both types of catalysts. Our studies showed that, for the first time, although the PtRh–SnO_2 with a PtRh alloy core was still active, the formation of a partially oxidized Pt and Rh core coincides with a 2.5-fold increase in the CO_2 generation rate for EOR.

Carbon-supported $PtRhO_x$–SnO_2 nanoparticles with a partially oxidized Pt and Rh core and SnO_2 shell were synthesized by a "surfactant-free" polyol process using $NaPtCl_4{\cdot}xH_2O$, $K_3RhCl_6{\cdot}xH_2O$, and $SnCl_2$ as precursors in an ethylene glycol solution (see the Supporting Information). PtRh–SnO_2 nanoparticles with a PtRh alloy core and a SnO_2 shell were synthesized by heating $PtRhO_x$–SnO_2 nanoparticles under a reducing atmosphere at an elevated temperature. The molar ratio between Pt and SnO_2 was kept as 1:1, while the ratio between Pt and Rh was varied from 2:1 to 4:1. Table S1 (in the Supporting Information) summarizes the results from energy-dispersive X-ray spectroscopy measurements of the resulting catalysts, confirming the atomic ratio of Pt/Rh/Sn as 37:20:43 and 39:12:49.

Figure 1 shows transmission electron microscopy (TEM) images of the as-made and reduced carbon-supported $Pt_{37}/Rh_{20}/Sn_{43}$ nanoparticles with average sizes of 2.8 ± 0.9 nm and 6.5 ± 0.9 nm, respectively. TEM images of the as-made and reduced $Pt_{39}/Rh_{12}/Sn_{49}$ nanoparticles are shown in Figure S1 in the Supporting Information. The large size of the reduced samples was a result of coalescence of nanoparticles during the thermal treatment (H_2/Ar at 250 °C). Figures 1c and d show the scanning transmission electron microscope-electron energy loss spectroscopy (STEM-EELS) line scans of a typical as-made $Pt_{37}/Rh_{20}/Sn_{43}$ particle. The data show that Sn displayed a strong signal at the edges of the particle, whereas Pt displayed a strong signal in the center. The data provide unambiguous evidence for the core–shell structure with a Pt-rich core and Sn-rich shell in a heterogeneous structure on the atomic scale. The ionization energy of the Rh $M_{4/5}$-edge is in the range 307–312 eV energy loss, which is unfortunately overlapped by the residual signal from carbon K-edge. Therefore, the EELS line scan was unable to measure the distribution of Rh within the catalysts, though the EDS spectra showed the

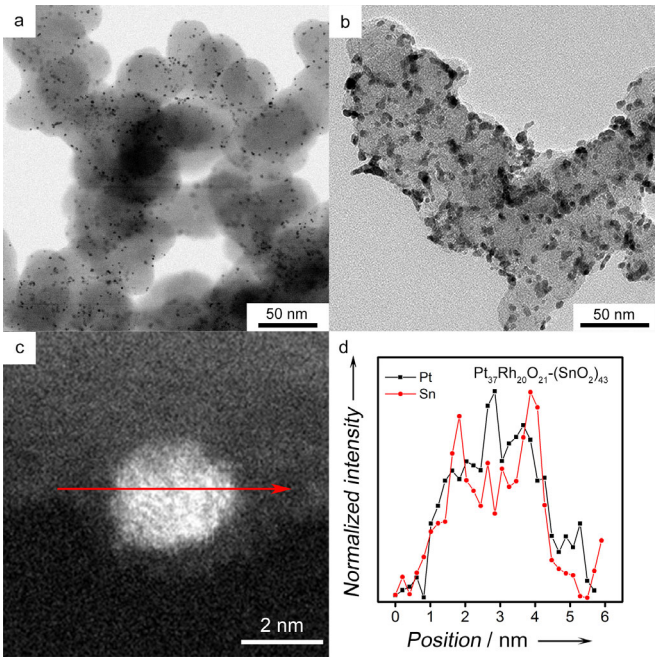

Figure 1. TEM images of (a) $Pt_{37}Rh_{20}O_x$–$(SnO_2)_{43}$/C and (b) $Pt_{37}Rh_{20}$–$(SnO_2)_{43}$/C. (d) EELS line scan across $Pt_{37}Rh_{20}O_x$–$(SnO_2)_{43}$ particle as indicated by the arrow in (c).

existence of Rh with appropriate chemical composition close to the ratio of the precursors. The X-ray diffraction (XRD) patterns of the as-made and reduced Pt/Rh/Sn samples are shown in Figure S2 in the Supporting Information. All the diffraction peaks could be assigned to the (111), (200), (220), (311), and (222) planes of a face centered cubic (fcc) structure. Diffraction peaks of SnO_2 were not observed in the as-made or reduced samples, although the STEM-EELS line scan showed Sn-rich shells in both samples. This could be attributed to the fact that Sn or SnO_2 existed in the form of very small nanoparticles or as an amorphous phase.

X-ray absorption (XAS) measurements were used to investigate the electronic states and local atomic environment of the Pt, Rh, and Sn in the as-made and reduced $Pt_{37}/Rh_{20}/Sn_{43}$ catalysts. Figure S3 (in the Supporting Information) shows the XAS data of the K-edges of Sn and Rh, and L_3-edge of Pt of the Pt/Rh/Sn catalysts, together with the standard materials such as metallic Sn, Pt, and Rh foils, as well as their oxides SnO_2, PtO_2, and Rh_2O_3. Figure S3a shows that the Sn K-edge data of the as-made and reduced Pt/Rh/Sn were very similar to those of SnO_2, suggesting that Sn was predominantly oxidized in all Pt/Rh/Sn samples. Combined with the structural information obtained by STEM-EELS, it has been suggested that SnO_2 primarily existed as a shell in both the as-made and reduced samples. On the other hand, the Pt L_3- and Rh K-edge absorption data suggested that Pt and Rh had very different electronic structures between the reduced and as-made samples (Figures S3b and c). For the reduced samples, Pt and Rh existed as predominantly metallic phase, evident from the similar white line (the intense peak at the K absorption edge) compared with their metal foil counterparts. For the as-made catalysts, Pt and Rh data resembled those of PtO_2 and Rh_2O_3,

indicating the existence of oxidized phases, although there were still discernable metallic Pt and Rh phases observed in both the as-made samples.

The Fourier transform magnitudes of extended X-ray absorption fine structure (EXAFS) data and theoretical fits for Pt, Sn, and Rh of Pt/Rh/Sn catalysts are shown in Figure S3 and Table S3 in the Supporting Information. The best-fit values of coordination numbers of $Pt_{37}/Rh_{20}/Sn_{43}$ are summarized in Table 1. For the reduced sample, the obtained first-nearest-

Table 1. EXAFS fitting results of Pt/Rh/Sn.

	Pt foil	Rh foil	$Pt_{37}Rh_{20}$–$(SnO_2)_{43}$	$Pt_{37}Rh_{20}O_x$–$(SnO_2)_{43}$
N_{Pt-Pt}	12		3.7 ± 0.5	7.4 ± 1.5
N_{Pt-Rh}			2.5	0
N_{Pt-M}			6.2 ± 0.5	
N_{Pt-O}			0	1.2 ± 0.5
N_{Rh-Rh}		12	4.7 ± 1.1	1.7 ± 1.1
N_{Rh-Pt}			4.6 ± 0.6	0
N_{Rh-M}			9.3 ± 1.6	
N_{Rh-O}			0.9 ± 0.6	2.2 ± 0.6
N_{Sn-Sn}			5.8 ± 2.5	0
N_{Sn-O}			3.3 ± 0.4	4.9 ± 0.5

neighbor Pt–metal ($N_{Pt-M} = N_{Pt-Pt} + N_{Pt-Rh}$) and Rh–metal ($N_{Rh-M} = N_{Rh-Rh} + N_{Rh-Pt}$) coordination numbers all had reasonably similar values within the uncertainties (6.2 ± 0.5 and 9.3 ± 1.6, respectively). That fact, and the other observation that the Pt–Rh and Rh–Pt contributions were required for both Pt and Rh edge analyses, in addition to the Pt–Pt and Rh-Rh contributions, respectively, demonstrated unambiguously the formation of a Pt–Rh alloy. For the as-made sample, however, Pt and Rh appeared to be the segregated phases without alloy formation, as evident from the fact that only Pt–Pt ($N_{Pt-Pt} = 7.4 \pm 1.5$) and Rh–Rh ($N_{Rh-Rh} = 1.7 \pm 1.1$) coordination was observed without any Pt–Rh and Rh–Pt coordination. Moreover, discernable Pt–O and Rh–O coordination indicated the existence of oxidized Pt and Rh phases. Strong Pt–Pt and Rh–Rh coordination, weak but discernable Pt–O and Rh–O coordination, and non-detectable Pt–Sn and Rh–Sn coordination corroborated well with the XANES analyses, concluding that the as-made $Pt_{37}/Rh_{20}/Sn_{43}$ catalysts were comprised of partially oxidized Pt and Rh cores.

Independent evidence towards similar conclusions could be concluded from the bond lengths. Table S3 indicates that Pt and Rh exist mainly in the metallic phase in the reduced $Pt_{37}/Rh_{20}/Sn_{43}$ sample, compared with as-made one. In the former sample, the Pt–Pt bond length (2.73 ± 0.01 Å) and Rh–Rh bond length (2.68 ± 0.01 Å) are similar to that in pure Pt (2.764 ± 0.003 Å) and Rh (2.685 ± 0.002 Å). In the as-made sample, the Pt–Pt bond length (2.67 ± 0.01 Å) and Rh–Rh bond length (2.80 ± 0.03 Å) are rather different from pure metallic Pt and Rh. In addition, the strong Sn–O coordination from both the as-made and reduced samples suggested the formation of tin oxide clusters, which is confirmed by the results obtained independently from STEM-EELS and XANES. Therefore, we concluded the coexistence of the biphase throughout the reduced $Pt_{37}/Rh_{20}/Sn_{43}$ catalyst, expressed as $Pt_{37}Rh_{20}$–$(SnO_2)_{43}$: a homogenous alloy core containing Pt and Rh, and SnO_2 clusters segregated on the shell; whereas the as-made sample showed a triphase feature expressed as Pt_{37}–Rh_{20}–O_x–$(SnO_2)_{43}$: a partially oxidized Pt and Rh core with segregated Pt and Rh phases, and SnO_2 clusters on the shell. Similar structural details can also be found in as-made and reduced $Pt_{39}/Rh_{12}/Sn_{49}$ catalysts (Figure S3, Table S3). Moreover, the degree of oxidation (value of x) for both Pt and Rh components in Pt_{37}-Rh_{20}-O_x-$(SnO_2)_{43}$ catalysts can be estimated by following equation:

$$x = \frac{N_{Pt-O} + N_{Rh-O}}{N_{Pt-Pt} + N_{Rh-Rh}} \times (37 + 20) = \frac{1.2 + 2.2}{7.4 + 1.7} \times 57 = 21 \qquad (1)$$

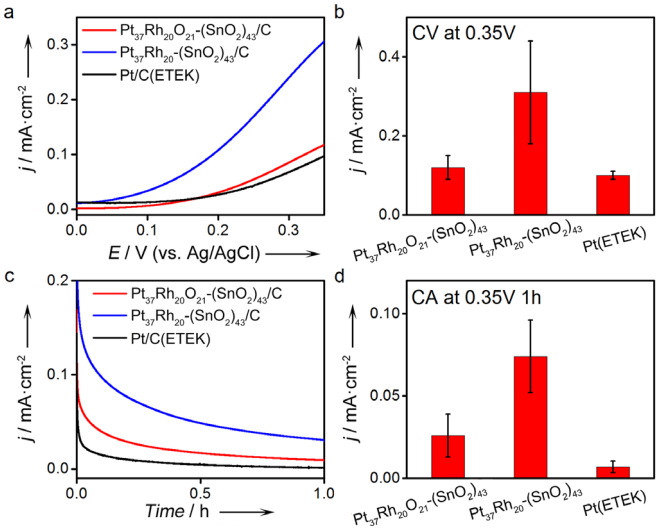

Figure 2. Electrochemical performance of carbon-supported $Pt_{37}Rh_{20}O_x$–$(SnO_2)_{43}$, $Pt_{37}Rh_{20}$–$(SnO_2)_{43}$, and Pt (ETEK) catalysts from (a, b) CVs and (c, d) CAs measurements.

Therefore, the exact formula of partially oxidized catalysts can be expressed as $Pt_{37}Rh_{20}O_{21}$–$(SnO_2)_{43}$.

The electrochemical activities of carbon-supported as-made $Pt_{37}Rh_{20}O_x$–$(SnO_2)_{43}$, its reduced counterpart $Pt_{37}Rh_{20}$–$(SnO_2)_{43}$, and commercial Pt/C were tested in a half-cell. Figure S4a (in the Supporting Information) shows the cyclic voltammograms (CVs) for the catalysts measured in 0.5 M H_2SO_4, from which the hydrogen absorption region was used to calculate the electrochemically active surface area (ECASA; Table S2 in the Supporting Information). Figure 2a shows the CV analyses of various catalysts measured in 0.5 M H_2SO_4 and 0.5 M ethanol electrolyte at a scan rate of 50 mV s^{-1} in the half-cell. The reduced catalyst exhibited superior current density, normalized by its ECASA. The current densities at 0.35 V obtained from CVs measurement are shown in Figure 2b; these follow the order: $Pt_{37}Rh_{20}$–$(SnO_2)_{43}$ > $Pt_{37}Rh_{20}O_{21}$–$(SnO_2)_{43}$ > Pt. The same order was also observed from chronoamperometry measurements (CAs) as shown in Figures 2c and d. These results indicated that $Pt_{37}Rh_{20}$–$(SnO_2)_{43}$ with a metallic PtRh alloy core increased the overall charge-transfer kinetics of the EOR. The high current density observed for the

$Pt_{37}Rh_{20}$–$(SnO_2)_{43}$ catalysts could be attributed to the bifunctional effect as the Pt/Rh atoms provide active sites for dehydrogenation of ethanol, whereas Sn provides oxygenated species to oxidize the intermediates. Such synergistic interactions make $Pt_{37}Rh_{20}$–$(SnO_2)_{43}$ a better catalyst with fast kinetics for adsorption and dehydrogenation of ethanol molecule.

To better understand the reaction mechanism, especially CO_2 generation by C–C splitting of ethanol during the EOR, we designed a four-electrode electrochemical cell (see the schematic of the cell in Figure S5 in the Supporting Information), including reference, working, and counter electrodes, and a CO_2 microelectrode. CV measurements with a scan rate of 0.5 mV s^{-1} were conducted for the EOR by using the four-electrode cell (Figure S6a in the Supporting Information). In addition, the CO_2 partial pressure (P_{CO2}) was measured simultaneously by the CO_2 microelectrode (Figure S6b). The total amount of CO_2 generation N_{CO2} was then calculated, as well as the generation rate of CO_2. The current density resulting from the generation of CO_2 (j_{CO2}) is expressed as:

$$j_{CO2} = \frac{dN_{CO2}}{dt} \times 6 \times F \quad (2)$$

where F is the Faraday constant, and 6 represents the number of electrons transferred upon forming one CO_2 molecule. Finally, the selectivity of CO_2 generation versus byproduct generation (e.g., CH_3CHO, CH_3COOH) is calculated by:

$$CO_2 \text{ selectivity} = \frac{j_{CO_2}}{j_{Total} - j_{CO_2}} \quad (3)$$

where j_{Total} is the total current, obtained from CV measurements, which represents the current resulting from the formation of all products.

Many studies have been reported on the CO_2 generation in situ by using Fourier transform infrared spectroscopy, differential electrochemical mass spectrometry, or gas chromatography,[24,25] from which the concentrations of CO_2 as a function of potential were presented. However, to the best of our knowledge, the electrokinetic details of CO_2 formation, such as CO_2 generation rate and/or selectivity of CO_2 generation have not been reported. Thanks to the high sensitivity (towards CO_2 concentration of 0.2 μM) and short data acquisition time (five seconds) of the CO_2 microelectrode, in this study we were able to provide comprehensive electrokinetic details of CO_2 generation by C–C splitting, which has never been reported before. Figure 3a shows the partial pressure of CO_2 recorded simultaneously during the CV measurements by using CO_2 microelectrode. $Pt_{37}Rh_{20}O_{21}$–$(SnO_2)_{43}$ showed 2.2 and 3.3 times higher P_{CO2}, as well as a 2.5 times higher CO_2 generation rate than $Pt_{37}Rh_{20}$–$(SnO_2)_{43}$ and commercial Pt at 0.35 V as shown in Figure 3b. Also, the onset potential of CO_2 generation for

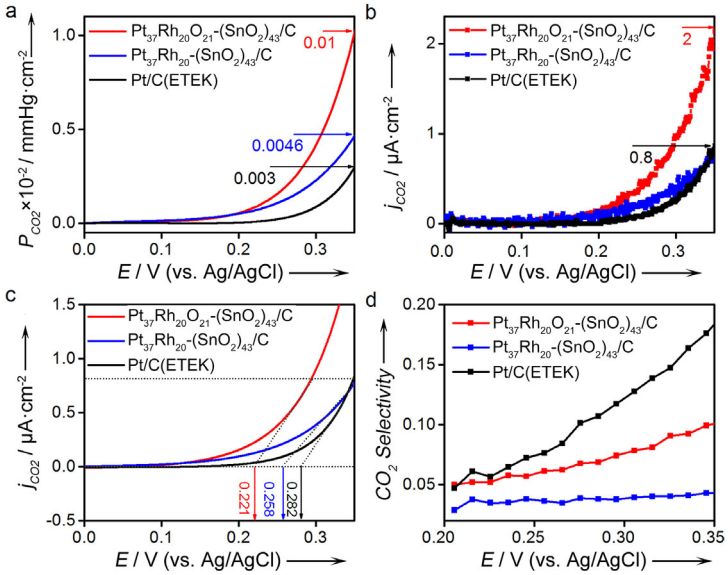

Figure 3. CO_2 generation by carbon-supported $Pt_{37}Rh_{20}O_x$–$(SnO_2)_{43}$, $Pt_{37}Rh_{20}$–$(SnO_2)_{43}$, and Pt (ETEK) catalysts during CV measurements, including (a) partial pressure (P_{CO2}), (b) current density resulting from CO_2 generation (j_{CO2}), (c) onset potential for CO_2 generation, and (d) CO_2 selectivity.

$Pt_{37}Rh_{20}O_{21}$–$(SnO_2)_{43}$, calculated through fitting Figure 3b (see details in Figure S8 in the Supporting Information), was about 37 and 61 mV lower than that of $Pt_{37}Rh_{20}$–$(SnO_2)_{43}$ and commercial Pt as shown in Figure 3c. Figure 3d shows that $Pt_{37}Rh_{20}O_{21}$–$(SnO_2)_{43}$ displayed higher CO_2 selectivity than $Pt_{37}Rh_{20}$–$(SnO_2)_{43}$ from 0.2 V to 0.35 V, demonstrating 2.8 times higher CO_2 selectivity at 0.35 V. These results showed that CO_2 generation by C–C bond splitting of ethanol was enhanced on the triphasic $Pt_{37}Rh_{20}O_{21}$–$(SnO_2)_{43}$ with a partially oxidized Pt and Rh core. Notably, although $Pt_{37}Rh_{20}O_{21}$–$(SnO_2)_{43}$ displayed a superior CO_2 generation rate, commercial Pt has the highest CO_2 selectivity, largely owing to the low overall current density (j_{Total}).

In addition to the discovery of an unexpected promotional effect of the partially oxidized Pt and Rh core on the CO_2 generation, we also found that the chemical composition of Pt and Rh played a role in electrokinetics of CO_2 generation. Pt/Rh/Sn materials with different Pt and Rh compositions were synthesized, indexed as $Pt_{39}/Rh_{12}/Sn_{49}$. Our electrochemical data showed similar results: in terms of CO_2 generation, $Pt_{39}/Rh_{12}/Sn_{49}$ underperforms $Pt_{37}/Rh_{20}/Sn_{43}$ (Figure S6, Figure S7, Table S2 in the Supporting Information), but triphasic $Pt_{39}Rh_{12}O_{21}$–$(SnO_2)_{49}$ with a partially oxidized Pt and Rh core indeed outperformed biphasic $Pt_{39}Rh_{12}$–$(SnO_2)_{49}$ with a PtRh alloy core. The former suggests a Pt to Rh ratio of nearly 2:1 was the optimal composition for CO_2 generation, and the latter confirms that a partially oxidized Pt and Rh core has better CO_2 generation kinetics than the PtRh alloy core.

The exact mechanism of the promotional effect of the partially oxidized Pt and Rh core found in $Pt_{37}Rh_{20}O_{21}$–$(SnO_2)_{43}$ on the CO_2 generation kinetics by C–C splitting is still under investigation. However, it is clear that the ensemble effect, associated with the particular arrangements of the Pt, Rh, and

O constituents, plays an important role in the C–C splitting of ethanol. In lieu of ethanol dissociation, co-existing metallic and oxidized Pt and Rh might show a special advantage for C–C splitting. According to DFT calculations conducted on the process of $CO + {}^{1}/_{2}\,O_2 \rightarrow CO_2$, the reaction barrier to CO_2 formation is significantly lower if O atoms from the edge of the surface oxide are involved in the CO oxidation, compared with the reaction only involving chemisorbed O atoms.[22] Thus, co-existence of metallic and oxidized Pt and Rh on the surface is expected to facilitate CO_2 formation, whereas the metallic phase provides a large and available site for dissociative adsorption of ethanol by C–C splitting and the oxidized Pt and Rh phases provide mobile O atoms for the oxidation of reaction intermediates such as CO and CH_x. Our findings for the partially oxidized core–shell catalysts, $Pt_{37}Rh_{20}O_{21}$–$(SnO_2)_{43}$, are of major importance for understanding the complete electro-oxidation of ethanol on a fundamental level, and will aid in the design of a new genre of electrocatalysts that have a partially oxidized noble metal core for various reactions.

Acknowledgments

This material is based upon work supported by the National Science Foundation (CHE 1152771). Use of the NSLS was supported by the U.S. Department of Energy. The authors acknowledge the facilities support provided at the Synchrotron Catalysis Consortium (U.S. Department of Energy, Grant No. DE-SC0012335). STEM-EELS was carried out at the Center for Functional Nanomaterial at Brookhaven National Laboratory supported by U.S. Department of Energy, Office of Basic Energy Sciences.

Keywords: core–shell structures · electrocatalysis · ethanol · platinum · rhodium

[1] X. H. Xia, H. D. Liess, T. Iwasita, *J. Electroanal. Chem.* **1997**, *437*, 233.
[2] M. H. Shao, R. R. Adzic, *Electrochim. Acta* **2005**, *50*, 2415.
[3] H. Hitmi, E. M. Belgsir, J. M. Leger, C. Lamy, R. O. Lezna, *Electrochim. Acta* **1994**, *39*, 407.
[4] M. J. Giz, G. A. Camara, *J. Electroanal. Chem.* **2009**, *625*, 117.
[5] H. Wang, Z. Jusys, R. J. Behm, *J. Phys. Chem. B* **2004**, *108*, 19413.
[6] G. A. Camara, T. Iwasita, *J. Electroanal. Chem.* **2005**, *578*, 315.
[7] W. X. Du, Q. Wang, C. A. LaScala, L. H. Zhang, D. Su, A. I. Frenkel, V. K. Mathur, X. W. Teng, *J. Mater. Chem.* **2011**, *21*, 8887.
[8] A. Kowal, M. Li, M. Shao, K. Sasaki, M. B. Vukmirovic, J. Zhang, N. S. Marinkovic, P. Liu, A. I. Frenkel, R. R. Adzic, *Nat. Mater.* **2009**, *8*, 325.
[9] M. Li, D. A. Cullen, K. Sasaki, N. S. Marinkovic, K. More, R. R. Adzic, *J. Am. Chem. Soc.* **2013**, *135*, 132.
[10] M. Li, W. P. Zhou, N. S. Marinkovic, K. Sasaki, R. R. Adzic, *Electrochim. Acta* **2013**, *104*, 454.
[11] N. Erini, R. Loukrakpam, V. Petkov, E. A. Baranova, R. Z. Yang, D. Teschner, Y. H. Huang, S. R. Brankovic, P. Strasser, *ACS Catal.* **2014**, *4*, 1859.
[12] E. A. de Souza, M. J. Giz, G. A. Camara, E. Antolini, R. R. Passos, *Electrochim. Acta* **2014**, *147*, 483.
[13] L. C. Silva-Junior, G. Maia, R. R. Passos, E. A. de Souza, G. A. Camara, M. Janete Giz, *Electrochim. Acta* **2013**, *112*, 612.
[14] A. Bach Delpeuch, F. Maillard, M. Chatenet, P. Soudant, C. Cremers, *Appl. Catal. B* **2016**, *181*, 672.
[15] T. Sheng, W. F. Lin, C. Hardacre, P. Hu, *Phys. Chem. Chem. Phys.* **2014**, *16*, 13248.
[16] J. M. Jin, T. Sheng, X. Lin, R. Kavanagh, P. Hamer, P. J. Hu, C. Hardacre, A. Martinez-Bonastre, J. Sharman, D. Thompsett, W. F. Lin, *Phys. Chem. Chem. Phys.* **2014**, *16*, 9432.
[17] W. X. Du, G. X. Yang, E. Wong, N. A. Deskins, A. I. Frenkel, D. Su, X. W. Teng, *J. Am. Chem. Soc.* **2014**, *136*, 10862.
[18] K. Qadir, S. H. Joo, B. S. Mun, D. R. Butcher, J. R. Renzas, F. Aksoy, Z. Liu, G. A. Somorjai, J. Y. Park, *Nano Lett.* **2012**, *12*, 5761.
[19] M. E. Grass, Y. Zhang, D. R. Butcher, J. Y. Park, Y. Li, H. Bluhm, K. M. Bratlie, T. Zhang, G. A. Somorjai, *Angew. Chem. Int. Ed.* **2008**, *47*, 8893; *Angew. Chem.* **2008**, *120*, 9025.
[20] Z. Duan, G. Henkelman, *ACS Catal.* **2014**, *4*, 3435.
[21] M. D. Ackermann, T. M. Pedersen, B. L. M. Hendriksen, O. Robach, S. C. Bobaru, I. Popa, C. Quiros, H. Kim, B. Hammer, S. Ferrer, J. W. M. Frenken, *Phys. Rev. Lett.* **2005**, *95*, 255505.
[22] R. Westerström, J. G. Wang, M. D. Ackermann, J. Gustafson, A. Resta, A. Mikkelsen, J. N. Andersen, E. Lundgren, O. Balmes, X. Torrelles, J. W. M. Frenken, B. Hammer, *J. Phys. Condens. Matter* **2008**, *20*, 184018.
[23] R. F. B. De Souza, J. C. M. Silva, M. H. M. T. Assumpção, A. O. Neto, M. C. Santos, *Electrochim. Acta* **2014**, *117*, 292.
[24] J. Gomes, D. Profeti, L. J. Deiner, *ChemElectroChem* **2014**, *1*, 655.
[25] J. Yin, S. Shan, M. S. Ng, L. Yang, D. Mott, W. Fang, N. Kang, J. Luo, C.-J. Zhong, *Langmuir* **2013**, *29*, 9249.

Received: April 13, 2016
Published online on ■■ ■■, 0000

*G. Yang, A. I. Frenkel, D. Su, X. Teng**

■■ – ■■

Enhanced Electrokinetics of C–C Bond Splitting during Ethanol Oxidation by using a Pt/Rh/Sn Catalyst with a Partially Oxidized Pt and Rh Core and a SnO_2 Shell

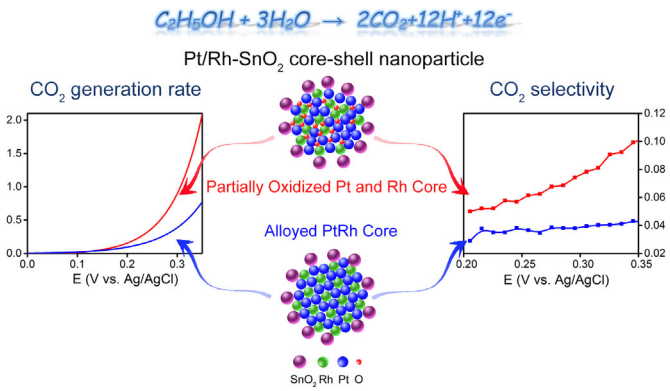

A partially oxidized Pt and Rh core with a SnO_2 shell exhibited a much higher CO_2 generation rate and CO_2 selectivity than the PtRh alloyed core with SnO_2 shell towards the electro-oxidation of ethanol.